AIAA JOURNAL
Vol. 44, No. 11, November 2006

Computational Fluid Dynamics Driven Optimization of Blended Wing Body Aircraft

Sergey Peigin*
Israel Aircraft Industries, Ben-Gurion Airport, 70100, Israel
and
Boris Epstein†
Academic College of Tel-Aviv Yaffo, 64044 Tel-Aviv, Israel

DOI: 10.2514/1.19757

The blended wing body aircraft has aroused considerable interest as a potential candidate for future large subsonic transport air vehicles. In this paper, we present the results of one- and multipoint multiconstrained optimization of a blended wing body configuration for minimum total drag. The optimization technique includes a new strategy for efficient handling of nonlinear constraints in the framework of genetic algorithms, scanning of the optimization search space by a combination of full Navier–Stokes computations with reduced-order methods and multilevel parallelization of the whole computational framework. The assessment of the results shows that the proposed technology allows the design of feasible aerodynamic shapes that possess a low drag at cruise conditions, satisfy a large number of geometrical and aerodynamic constraints, and offer good off-design performance in markedly different flight conditions.

Nomenclature

C_D	=	total drag coefficient
C_L	=	total lift coefficient
C_M	=	total pitching moment coefficient
C_p	=	pressure coefficient
M	=	freestream Mach number
N_D	=	dimension of the search space
N_{ws}	=	number of sectional airfoils
Q	=	objective function
R/c	=	relative radius of the airfoil leading edge
Re	=	freestream Reynolds number
t/c	=	relative thickness of airfoil
w_k	=	weighting coefficients for multipoint optimization
α	=	angle of attack
$(\Delta y/c)$	=	relative local thickness of airfoil
θ	=	trailing-edge angle of airfoil

Superscript

b	=	baseline configuration value

I. Introduction

THE blended wing body (BWB) aircraft is a tailless design that integrates the wing and the fuselage. The conceptual advantage of this configuration lies in its lower wetted area to volume ratio and lower interference drag as compared with the conventional transport aircraft. A BWB has an additional advantage: lift and payload are much more in line. This reduces blending moments and therefore structural weight. The concept goes back to nonconventional flying wing designs originally proposed almost 60 years ago [1]. The BWB configuration concept is a radical change from the dominant design where a wing is combined with a cylinder-type fuselage, and the longitudinal stability of the aircraft is maintained by means of a tail.

In the late 1990s, the BWB aircraft was considered in the United States as a potential candidate for future large subsonic transport aircraft [2,3]. The project involved a number of industrial and academic establishments, including National Aeronautics and Space Administration (NASA). The comprehensive survey of these activities may be found in [4].

A serious effort was also mounted in Europe to design their version of a BWB configuration. Starting in 2002, a European commission funded a project aimed at the design and optimization of BWB aircraft [5]. A progressive study of the aerodynamic performance for the corresponding BWB configuration may be found in [6], where a BWB geometry without fins was considered.

It is the authors' opinion, that computational fluid dynamics (CFD) and CFD-driven optimization methods could play a great role in fulfilling the aerodynamic objectives of the above projects. The first optimization method in aerodynamics was that of Lighthill [7] which proposed to employ the conformal mapping for the design of two-dimensional airfoils. An alternate method that solves the potential equations in the hodograph plane was established by Bauer et al. [8]. Constrained optimization was considered by Hicks et al. [9] where the sensitivity derivatives were evaluated by finite differences. Numerous optimization tools are based on gradient approach [10]. Methods, developed by Jameson [11,12], compute the gradients from the solutions to the flow equations and its adjoint equations. The present state-of-the-art of this class of methods can be found in [13]. The design problem may be characterized by a mix of continuous, discrete and integer design variables, and the resulting design space can be nonconvex or even disjointed. For all these reasons, optimization methods that do not rely on the computation of gradients, in particular evolutionary programming and genetic algorithms (GAs), received a considerable growth of interest [14–16].

However, before the last few years, CFD-driven optimization had a limited impact on the aircraft design practice especially in the case of complex 3-D aerodynamic shapes similar to BWB.

The reason why the optimization tools are still not being exploited as one would like in the design process is partially due to the following three reasons. First, only recently computational simulation has been allowed for relatively accurate drag prediction (within the accuracy of 2–3 aerodynamic counts) required in engineering practice (see the results of the 2nd AIAA Drag

Received 30 August 2005; revision received 30 June 2006; accepted for publication 12 July 2006.

*Professor, Engineering Division; speigin@iai.co.il. Member AIAA.
†Professor, Computer Science Department; epstein@mta.ac.il. Member AIAA.

Prediction Workshop[‡]). Second, the industrial optimization of aerodynamic shapes necessitates high-dimensional search spaces, and a large number of nonlinear constraints are placed upon a desired optimum.

Last but not least, the huge computational volume needed for optimization (and the corresponding huge computational resources) presents a major obstacle to the incorporation of CFD-based optimization into the core of the industrial aerodynamic design.

The aerodynamic optimization of BWB configurations presents additional difficulties compared with the optimization of conventional aircraft configurations due to an essential increase in the number of design variables and to the necessity to comply with a number of additional aerodynamic constraints coming from the stability considerations.

In [17] an efficient and robust algorithm for CFD-driven optimization of three-dimensional aerodynamic wings, based on Genetic Algorithms search and full Navier–Stokes computations, was proposed by the authors. In this context, the main objective of this paper is to apply the method [17] to the one- and multipoint multiconstrained optimization of a BWB configuration for minimum total drag, and to analyze the influence of the aerodynamic parameters of the problem on the optimal configuration. It was demonstrated that the optimization method allows the design of feasible aerodynamic shapes that possess a low drag at cruise conditions, satisfy a large number of geometrical and aerodynamic constraints and offer good off-design performance in markedly different flight conditions such as takeoff conditions and high Mach zone.

II. Statement of the Problem

In the design practice, the parameters of optimization originate from the conceptual design stage which provides the initial geometry definition and the aerodynamic performance data. The aerodynamic specification includes the prescribed cruise lift, Mach number, altitude, and maximum allowed drag values that will meet the goals of the aircraft mission (such as range, payload, fuel volume, etc.).

The desired optimal geometry is sought from a class of solutions that satisfy different geometrical, aerodynamic, and multidisciplinary constraints (which also originate from the stage of conceptual design). Specifically, airfoil thickness, pitching moment, $C_L^{\max}$ at the takeoff conditions are normally constrained.

The design objective is to develop an aircraft configuration with as low a drag at cruise conditions as possible which, at the same time, satisfies the above constraints. This is accomplished through a CFD-based solution of the properly formulated multipoint constrained optimization problem.

In the problem formulation, the first crucial issue is the choice of the objective function. We assume that the drag coefficient C_D of a configuration (at constant reference area) is a sensitive and reliable indicator of its aerodynamic performance and thus we employ C_D as the objective function of the considered optimization problem.

The next important issue is the implementation of constraints in the optimization algorithm. Where possible, the constraints should be satisfied accurately (up to machine accuracy) and directly, whereas the remaining constraints should be converted into alternative constraints that can be expressed in terms of drag.

For example, we should satisfy the geometrical constraints and such aerodynamic constraints as the prescribed lift coefficient exactly whereas the requirement of a sufficiently high $C_L^{\max}$ at the takeoff conditions should be reformulated in terms of drag at the corresponding flight conditions. This means that instead of maximizing $C_L^{\max}$, we minimize C_D at a fixed C_L value close to that needed to meet the specified aerodynamic requirements.

Finally in order to ensure the accuracy of optimization we require that for any geometry feasible from the constraints' viewpoint, the value of the objective (cost) function remains exactly equal to the value of the drag coefficient without any penalization.

[‡]See http://www.cfdreview.com/articles/03/10/20/1357201.shtml [cited 10_May_2005].

Based on the above principles, the mathematical formulation of the optimization problem may be expressed as follows.

The objective of the general multipoint optimization problem is to minimize the weighted combination C_D^{wtd} of drag coefficients at the main design and secondary design points (flight conditions)

$$C_D^{\text{wtd}} = \sum_{k=1}^{K} w_k C_D(k)$$

where K is the total number of the design points. The specific values of the weight factors w_k reflect the relative importance of the design points coming from the aerodynamic practice. The main design point deals with cruise conditions. Secondary design points are chosen in order to ensure good off-design aerodynamic performance. Specifically, the following secondary design points may be used: 1) a higher Mach design point (to improve Mach drag rise behavior); 2) a higher C_L design point at the cruise Mach number (to improve climb behavior), and 3) a design point corresponding to the takeoff conditions.

The solution is sought in the class of wing shapes subject to the following classes of constraints:

1) Aerodynamic constraints such as prescribed constant total lift coefficient $C_L^*(k)$ and minimum allowed pitching moment $C_M^*(k)$:

$$C_L(k) = C_L^*(k), \qquad C_M(k) \geq C_M^*(k) \tag{1}$$

Thus we assume that $C_L^*(k)$ and $C_M^*(k)$ are not a function of design variables.

2) Geometrical constraints on the shape of the wing surface in terms of properties of sectional airfoils at the prescribed wing span locations: relative thickness $(t/c)_i$, relative local thickness $(\Delta y/c)_{ij}$ at the given chord locations $(x/c)_{ij}$ (beam constraints), relative radius of leading edge $(R/c)_i$, trailing-edge angle θ_i:

$$(t/c)_i \geq (t/c)_i^*, \qquad (\Delta y/c)_{ij} \geq (\Delta y/c)_{ij}^*, \qquad (R/c)_i \geq (R/c)_i^*$$
$$\theta_i \geq \theta_i^* \qquad i = 1, \ldots, N_{ws}, \qquad j = 1, \ldots, N_{\text{bc}}(i) \tag{2}$$

where N_{ws} is the total number of sectional airfoils' subject to optimization, $N_{\text{bc}}(i)$ is the total number of beam constraints at section i, and values $(t/c)_i^*$, $(\Delta y/c)_{ij}^*$, θ_i^*, $(R/c)_i^*$, C_L^*, and C_M^* are prescribed parameters of the problem. Though only the above listed constraints were taken into account in the present work, it is possible (in the framework of the proposed method) to impose additional geometrical constraints, such as minimum allowed wing volume.

Thus in the present work the total number of considered constraints N_{cs} is equal to

$$N_{\text{cs}} = 2 \times K + 3 \times N_{ws} + \sum_{i=1}^{N_{ws}} N_{\text{bc}}(i)$$

III. Optimization Method

A. CFD Driver

As a CFD driver of the optimization process the numerical solution of the full Navier–Stokes equations is used.

The use of a consistently accurate Navier–Stokes solver is a necessary requirement imposed upon any accurate optimization of aerodynamic shapes. Note that the optimization method requires not only the exact evaluations of the objective function (in our case, the total drag), but also accurate evaluations of additional sensitive aerodynamic characteristics needed in order to satisfy the aerodynamic constraints.

To do this, the numerical noise must be significantly lower than, for example, the difference in the values of drag for geometrically close but distinctly different aerodynamic shapes tested in the process of optimization.

The failure to fulfill the above requirement leads to the incorrect estimation of shapes in terms of the objective function (regardless of

the optimization technique) and thus may result in the failure of the whole optimization process.

In the present work, numerical solutions of the full Navier–Stokes equations are obtained by means of the multiblock code NES [18]. The numerical method employs structured point-to-point matched grids and is based on the essentially nonoscillatory (ENO) concept with a flux interpolation technique [19] that allows accurate estimation of sensitive aerodynamic characteristics such as lift, pressure drag, friction drag and pitching moment. The code ensures high accuracy of the Navier–Stokes computations, possesses high robustness for a wide range of flows and geometrical configurations and thus keeps the numerical noise to the low level [20].

The important advantage of the solver NES as a driver of the optimization process is its ability to supply reliable and sufficiently accurate results already on relatively coarse meshes (usually 4–8 times coarser than the ultimately resolved mesh) and thus to reduce dramatically the volume of CFD computations.

B. Optimum Search Strategy

The present optimization technique [17,21], is based on the use of genetic algorithms. As a basic algorithm, a variant of the floating-point GA [22] is used. The floating-point GAs realize a compromise between binary-coded GAs and evolution strategies, because they use most of the classical GAs mechanisms, whereas, they work directly at the phenotypic level like evolution strategies [23]. The mating pool is formed through the use of tournament selection [24]. This allows for an essential increase in the diversity of the parents. We employ the arithmetical crossover and the nonuniform real-coded mutation in a distance-dependent form [25]. To improve the convergence of the algorithm we also use the elitism principle, where the current best individual in the generation is automatically included in the next one.

In the considered optimization problem, the presence of constraints has a great impact on the solution. This is due to the fact that the optimal solution does not represent a local minimum in the conventional sense of the word. Instead, it is located on an intersection of hypersurfaces of different dimensions, generated by linear and nonlinear constraints [21]. Additionally, the problem of finding such an extremum is essentially complicated by the fact that these hypersurfaces, which bound the feasible search space, are not known in advance.

To make the optimum search efficient, we changed the conventional search strategy by employing search paths through both feasible and infeasible points. To implement the new strategy, it was proposed to extend the search space by evaluating (in terms of fitness) the points, which do not satisfy the constraints imposed by the optimization problem. A needed extension of an objective function may be implemented by means of GAs due to their basic property: contrary to classical gradient-based optimization methods, GAs are not confined to only smooth extensions (for more detail see [21]).

Based on this approach to the constraint handling, the modified objective function Q was defined as follows:

$$Q = \begin{cases} 0.1 + q_1 & \text{if } (t/c)_i < (t/c)_i^* \\ 0.125 + q_2 & \text{if } (\Delta y/c)_{ij} < (\Delta y/c)_{ij}^* \\ 0.15 + q_3 & \text{if } C_M < C_M^* \\ 0.2 + q_4 & \text{if } R_i < R_i^* \\ 0.3 + q_5 & \text{if } \theta_i < \theta_i^* \\ 0.5 + q_6 & \text{if } y_i^u(t) < y_i^l(t) \\ C_D & \text{otherwise} \end{cases} \tag{3}$$

$$\begin{aligned} q_1 &= [(t/c)_i^* - (t/c)_i] \\ q_2 &= [(\Delta y/c)_{ij}^* - (\Delta y/c)_{ij}] \\ q_3 &= [C_M^* - C_M] \\ q_4 &= [R_i^* - R_i] \\ q_5 &= [\theta_i^* - \theta_i] \\ q_6 &= 0 \end{aligned}$$

where each condition is tested independently for all i and j $[i = 1, \ldots, N_{ws}, j = 1, \ldots, N_{\text{bc}}(i)]$.

The choice of constants in Eq. (3) was fairly straightforward, based on the following principle. On the one hand, their values should be at least several times greater than the upper bound of C_D (about 0.0500 for the considered class of problems), which ensures that, for any feasible point, the value of the objective function will be low in comparison with that of any infeasible point. On the other hand, these constants should not be too high, in order to ensure that a sufficient number of infeasible points will be present in the population (as it was explained above).

In the case of multipoint optimization the value of C_D represents a weighted combination of total drag values at the flight points participating in optimization.

One of the main weaknesses of GAs lies in their poor computational efficiency. This prevents their practical use in the case where the evaluation of the cost function is computationally expensive as it happens in the framework of the full Navier–Stokes model. To overcome this, we introduce an intermediate "computational agent": a computational tool which, on the one hand is based on a very limited number of exact evaluations of objective function and, on the other hand provides a fast and reasonably accurate computational feedback in the framework of GAs search.

We construct a computational agent by means of a reduced-order models (ROM) approach in the form of local approximation method (LAM). With the ROM–LAM method, the solution functionals that determine a cost function and aerodynamic constraints (such as pitching moment, lift and drag coefficients), are approximated by a local data base. The data base is obtained by solving the full Navier–Stokes equations in a discrete neighborhood of a basic point (basic geometry) positioned in the search space. Note, that for the basic geometry, the design C_L is achieved by varying the angle of attack of the configuration.

So on the one hand, the number of exact estimations of the objective function (full Navier–Stokes solutions) is proportional to the dimension of the search space. On the other hand, the computational volume required to provide approximate estimates of the objective function in the framework of GAs optimum search, is negligible.

To overcome the approximate nature of the search, the search is simultaneously performed on a number of embedded search domains, and the set of thus obtained optimal shapes are verified through full Navier–Stokes evaluations.

Besides, in order to ensure the global character of the search, it is necessary to overcome the local nature of the above approximation. For this purpose it is suggested to perform iterations in such a way that in each iteration, the result of optimization serves as the initial point for the next iteration step (further referred to as optimization step). The specific algorithm is described in [17].

Additionally, multilevel parallelization of the whole optimization framework allows one to make use of the computational power supplied by massively parallel processors and thus to essentially improve the computational efficiency (for more detail see [26]).

C. Search Space Parameterization

In the present work the shape of the blended wing body is defined as follows:

1) Planview of the configuration is fixed.

2) The aircraft surface is generated by a linear spanwise interpolation between 2-D sectional cuts.

3) The number of the cuts N_{ws} is fixed.

4) Shape of the 2-D cuts is determined by Bezier Splines.

For the geometry description the absolute Cartesian coordinate system (x, y, z) is used, where the axes x and z are directed along the streamwise and span direction, respectively.

The aircraft planform is defined by the following parameters: the length c_1 at the symmetry plane $z = 0$, span location of the streamwise sections $\{z_i\}$, and the corresponding leading and trailing-edge sweep angles ($\{\lambda_i^{\text{le}}\}$ and $\{\lambda_i^{\text{tr}}\}$).

For each spanwise section, the nondimensional shape is defined in a local Cartesian coordinate system $(\bar{x}, \bar{y})$ in the following way. The coordinates of the leading edge and trailing edge were, respectively, (0, 0) and (1, 0). For approximation of the upper and lower cut surface, Bezier Spline representation was used. The choice for Bezier Splines was prompted by the previous experience with 2-D airfoil optimization [21]. It appeared that these splines possess good approximation properties while keeping a number of design variables to an acceptable level.

Finally, the shape of a sectional cut is completely determined by a total of $2N - 5$ parameters $(a_1, a_2, \ldots, a_{N-1}, a_N, \ldots, a_{2N-5})$, where N is the order of Bezier curve.

To fully specify the configuration shape it is necessary to set locations of the 2-D sectional cuts, in addition to their shapes. Assuming that the chord value and the trailing-edge location are defined by the planform, sectional locations are specified by means of two additional design parameters per section: twist angle $\{\alpha_i^{\text{tw}}\}$ and dihedral value $\{\gamma_i^{\text{dh}}\}$. Note that for the aircraft centerline section these values are set to zero. Summing up, the set of design parameters consists of Bezier spline coefficients, twist angle, and dihedral value for all design sections.

IV. Discussion of Results

In this section we present the results of one- and multipoint drag minimization of a blended wing body aircraft configuration without the influence of trailing-edge devices. The initial (tailless) geometry of the aircraft was proposed within the European Commission funded project [5] and may be found in [6]. The total aircraft span is equal to 77.5 m (compatible with existing airport runways). The leading edge sweep angles are swept back 63.8 deg for the center body and 38 deg for the outer wing, respectively. The trapezoidal wing area (842 m^2) is taken as the reference area. The length of the center chord is equal to 50.8 m. The number of spanwise cuts N_{ws} in the configuration definition was equal to 5. The cuts were located at the center line and $z = 13.0$, 17.5, 23.5, 38.75 m with a respective airfoils thickness of 18.0, 14.0, 10.0, 7.9, and 7.9%. The initial sectional shapes are extracted from the graphical data of [6]. The planform of the BWB aircraft is shown in Fig. 1.

The main design point was $C_L = 0.41$, $M = 0.85$ (as in [6]). The secondary design points were chosen at $M = 0.87$ (high Mach cruise conditions) and at $M = 0.2$ (takeoff conditions). The design Reynolds number was equal to 5.41×10^6 (assuming that the characteristic length in the Reynolds number definition is equal to 1 m). The geometrical constraints were imposed on thickness $[(t/c)_i^* = (t/c)_i^b]$, leading edge radius $[(R/c)_i^* = (R/c)_i^b]$ and trailing-edge angle $(\theta_i^* = \theta_i^b)$ as well as two local thickness constraints per section. An additional (aerodynamic) constraint was placed upon the pitching moment. The order of Bezier splines N was equal to 11. Thus, the total number of design variables N_D amounted to 93.

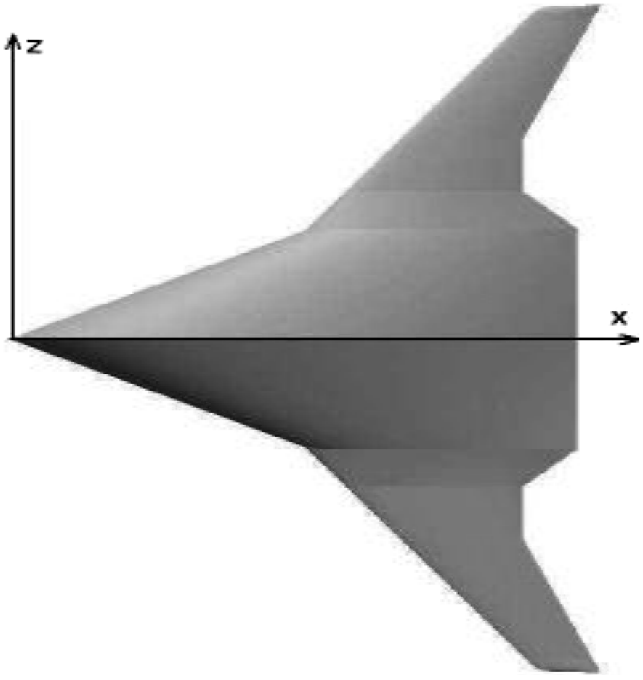

Fig. 1 BWB configuration: planform.

Table 1 Blended wing body aircraft: optimization conditions and constraints

Case no.	C_L^*	M	w_i	C_M^*
Case BWB_1	0.41	0.85	1.0	−0.300
Case BWB_2	0.41	0.85	1.0	−0.075
Case BWB_3	0.41	0.85	0.70	−0.075
	0.41	0.87	0.25	−0.100
	1.63	0.20	0.05	−0.330
Case BWB_4	0.41	0.85	0.95	−0.075
	1.63	0.20	0.05	−0.330

Table 2 Blended wing body aircraft: optimization results

Case	C_D (counts) at $M = 0.85$, $C_L = 0.41$	C_D (counts) at $M = 0.87$, $C_L = 0.41$	$C_L^{\max}$ at $M = 0.20$
Baseline	247.0	287.0	1.63
Case BWB_1	194.5	207.4	1.51
Case BWB_2	196.4	213.4	1.47
Case BWB_3	196.7	202.5	1.76
Case BWB_4	196.6	216.6	1.67

The design conditions and constraints are summarized in Table 1, whereas the results of optimization are given in Table 2. The corresponding optimal shapes are designated by case BWB_1 to case BWB_4.

Because the optimization algorithm is highly parallelized, a multiprocessor cluster is required for its implementation. Specifically at Israel Aircraft Industries, a cluster of MIMD (multiple instructions multiple data) multiprocessors consisting of 228 nodes was employed. Each node has 2 processors, 2 GB RAM memory, 512 KB level 2 cache memory and full duplex 100 Mbps Ethernet interface. Totally this cluster contained 456 processors with 456 GB RAM and 114 MB level 2 cache memory.

For the transonic BWB aircraft configuration, NES provides accurate asymptotically converged estimates of aerodynamic coefficients with the fine level grids containing $209 \times 57 \times 41$ computational points in the streamwise, spanwise, and normal to surface direction, respectively.

Unfortunately, such computations, though feasible for a single optimization, are too heavy to be used in the industrial framework. To overcome this limitation, we used the invariance of the hierarchy of objective function values on the medium and fine grids [17]. It is feasible if the grid coarsening preserves the hierarchy of fitness function values on the search space (that is, the relation of order is invariant with respect to grid coarsening). This means that the objective function Q_c defined on a coarse grid can be used for solution of the optimization problem, if for every pair of points x_1, x_2 belonging to the search space, the relation of order between the values of an objective function Q_c on a coarse grid implies the same order relation for the objective function Q_f defined on a fine grid. For 2-D optimization, the feasibility of the above approach was confirmed in [21].

It appeared that the 2 times coarser in each direction $(105 \times 29 \times 21)$ grids satisfy the invariance conditions. This allowed us to use meshes with such a resolution for optimization purposes.

One single-point optimization requires an overnight run on the above cluster whereas a typical three-point optimization which includes one main design point and two secondary design points, may take as much as 1.5–2 days.

Note, that though the CFD computations employed in the optimization stream were based on the medium grid resolution, all the aerodynamic data listed below were obtained on the fine grid.

A. One-Point Optimization

Before discussing the obtained results we compare the present results with other published results. The considered BWB aircraft configuration was the subject of a previous optimization within a European project [5]. The results of this single-point optimization at the main cruise conditions ($C_L = 0.41$, $M = 0.85$) were reported in [6]. In [6] the optimization with a gradient method, was based on the solution of the Euler equations and the corresponding adjoint equations [11], whereas the final optimal shape was verified through the solution of the full Navier–Stokes equations.

The comparison of the results in [6] with those obtained by the present method (one-point optimization case BWB_1) is as follows. In [6], the reduction of 26 aerodynamic counts was achieved (out of the initial 285.5 counts). The corresponding optimization by the present method yielded the reduction of 52.5 counts (out of the initial 247 counts).

To obtain a better assessment of the optimization results, it is worthwhile to analyze the aerodynamic behavior of the baseline BWB configuration (taken from [6]). A CFD analysis (performed by the code NES [18]) at transonic flight conditions provides evidence to strong shocks on most of the aircraft upper surface (see Figs. 2 and 3).

The computation at $C_L = 0.41$, $M = 0.85$ yields 247 counts. At this flight point, the theoretical induced drag (taking into account the difference between the wetted and the reference wing areas) is estimated to be about 75 counts. On the other hand, the zero lift total drag for the same configuration, for a purely subsonic flow at $M = 0.60$, is equal to 115 counts. Thus the baseline configuration possesses a fair amount of wave drag which gives a good promise that a proper shape optimization should result in a significant drag reduction. This conclusion may be also confirmed by the computation at $C_L = 0.41$, $M = 0.60$ where the total drag is equal to 190.6 counts, which complies with the previous wave drag estimate at the main design point (above 50 counts).

The first optimization case labeled as case BWB_1, is a single-point optimization with unconstrained pitching moment. The total drag of the optimal configuration amounts to 194.5 counts (compared with the initial 247.0 counts) with the pitching moment $C_M = -0.300$ compared with the baseline $C_M = -0.075$. The comparison of sectional pressure distributions for the baseline shape (Figs. 2 and 3) with the optimized ones for $M = 0.85$ (Figs. 4 and 5) shows that the original strong shock was virtually eliminated by the optimization. This resulted in a total drag level close to the above estimated low bound (about 191 aerodynamic counts). Note that the shock elimination phenomenon is not pointwise: this trend is also clearly observed at Figs. 6–9, where streamwise pressure distributions at a higher Mach value $M = 0.87$ are depicted.

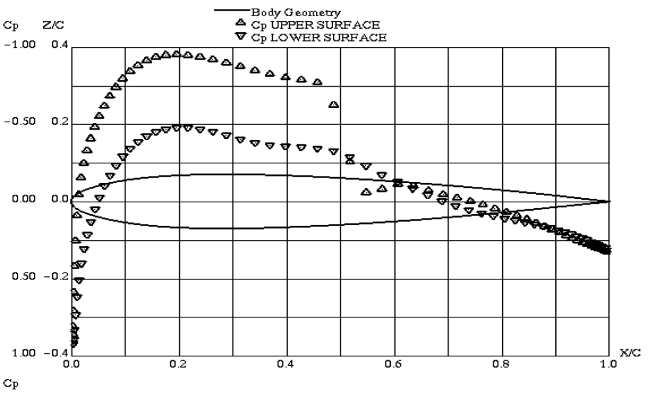

Fig. 2 BWB baseline configuration. Streamwise pressure distribution at section $z = 13.0$ m. $M = 0.85$, $C_L = 0.41$.

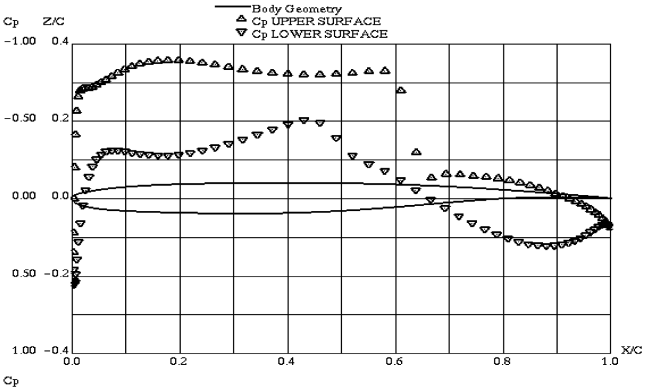

Fig. 3 BWB baseline configuration. Streamwise pressure distribution at section $z = 23.5$ m. $M = 0.85$, $C_L = 0.41$.

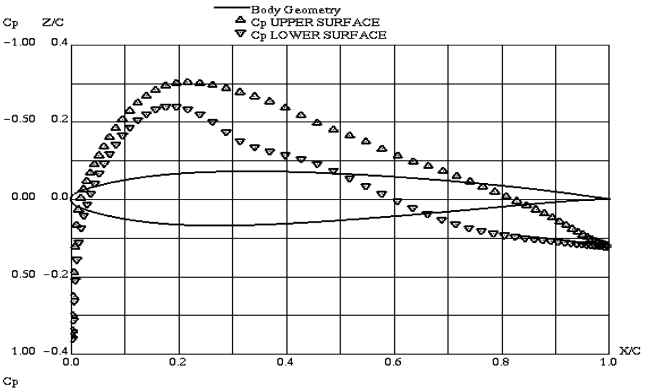

Fig. 4 BWB configuration. One-point optimization: case BWB_1. Streamwise pressure distribution at section $z = 13.0$ m. $M = 0.85$, $C_L = 0.41$.

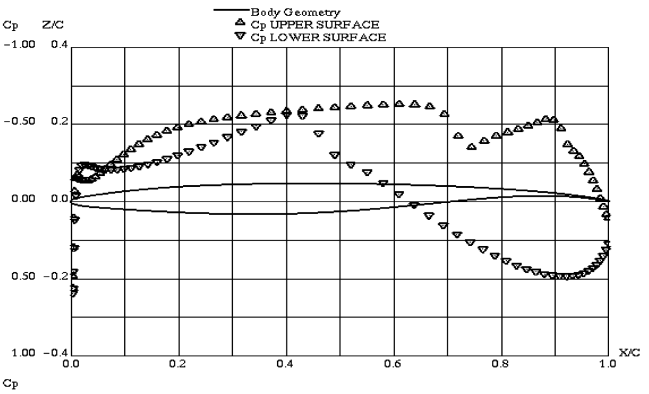

Fig. 5 BWB configuration. One-point optimization: case BWB_1. Streamwise pressure distribution at section $z = 23.5$ m. $M = 0.85$, $C_L = 0.41$.

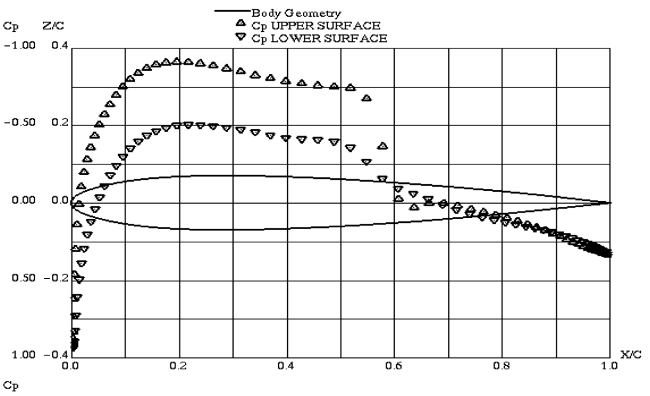

Fig. 6 BWB baseline configuration. Streamwise pressure distribution at section $z = 13.0$ m. $M = 0.87$, $C_L = 0.41$.

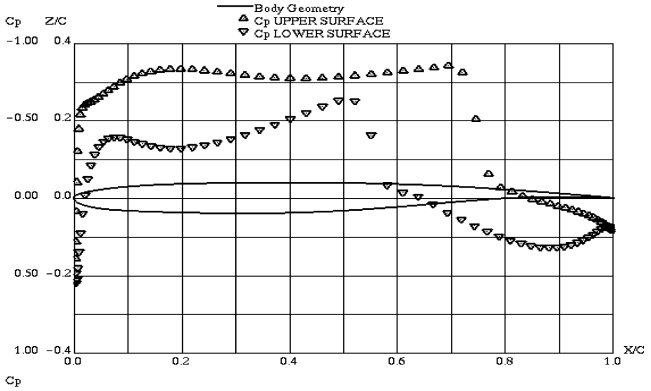

Fig. 7 BWB baseline configuration. Streamwise pressure distribution at section $z = 23.5$ m. $M = 0.87$, $C_L = 0.41$.

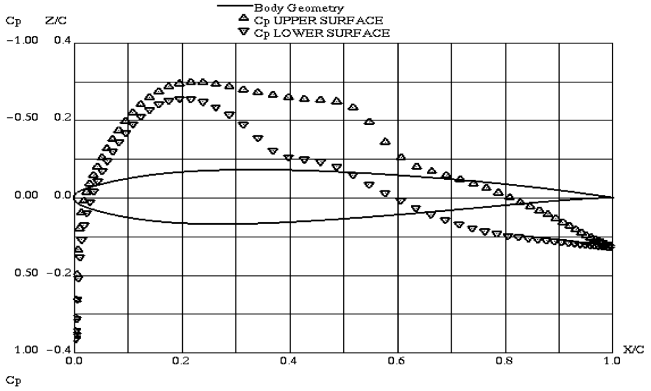

Fig. 8 BWB configuration. One-point optimization: case BWB_1. Streamwise pressure distribution at section $z = 13.0$ m. $M = 0.87$, $C_L = 0.41$.

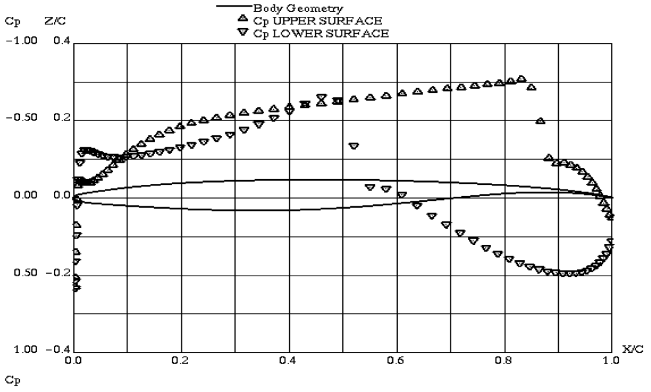

Fig. 9 BWB configuration. One-point optimization: case BWB_1. Streamwise pressure distribution at section $z = 23.5$ m. $M = 0.87$, $C_L = 0.41$.

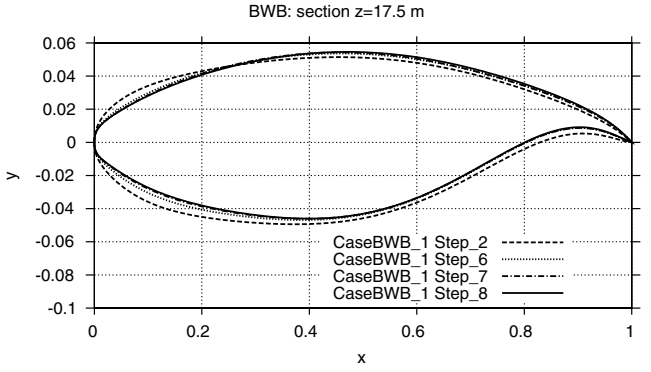

Fig. 10 BWB configuration. One-point optimization: case BWB_1. Shape of section at $z = 17.5$ m for different optimization steps.

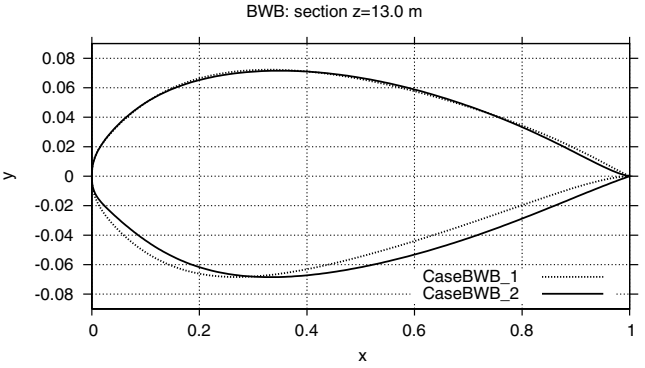

Fig. 11 BWB configuration. One-point optimizations. Shape of section at $z = 23.5$ m. Case BWB_1 vs case BWB_2.

The analysis of the iterative optimization stream (see Fig. 10) demonstrates that the main means of drag minimization is related to the build up of a highly cusped trailing-edge shape. Note that this trend is widely used in practical aerodynamic design.

At the same time, though the optimization (case BWB_1) was highly successful in terms of drag reduction, the corresponding C_M value appeared unacceptable due to stability considerations. This necessitated another one-point optimization (labeled case BWB_2) at the conditions of case BWB_1 with an additional constraint imposed on the pitching moment in order to keep it to the original level. The results of the optimization were as follows. The total drag was reduced to 196.4 counts, whereas the pitching moment of the optimal aircraft configuration was exactly equal to the original one ($C_M = -0.075$).

The analysis of the achieved results allows one to draw the following conclusions. First, the drag penalty due to the limitation of pitching moment amounted to only 1.9 counts. Second, though both optimal configurations yield very close total drag values, the corresponding shapes are markedly different (see Fig. 11). This may be explained in the following way. To comply with the constraint on the pitching moment, an essentially higher loading of the leading edge region of the aircraft (compared with the unconstrained optimization case BWB_1) should be achieved. This means that in this case, the drag minimization can not be accomplished by the same aerodynamic design techniques that were successfully used by the optimizer in case BWB_1. Indeed, as it can be seen from Fig. 11, the present optimization method discovered new aerodynamic resources and formed a drooped leading edge shape, which is another well known design feature.

B. Multipoint Optimization

From the pointwise optimization view, the results achieved in case BWB_2, are quite successful, because at the design conditions, the drag was reduced by 50.6 counts (coming close to the theoretical minimum) while keeping all the constraints (including that of the pitching moment) to the required level. However, the final decision on the feasibility of an optimal shape, should be made only upon the configuration testing at off-design conditions. Specifically, at least three following off-design characteristics should be checked. First, the drag behavior at higher-than-cruise lift conditions (at the cruise Mach value). Second, the quality of Mach drag divergence at the considered cruise $C_L = 0.41$. And finally, the value of $C_L^{\max}$ at the takeoff conditions should be tested.

With this end in view, the optimal BWB aircraft configuration (case BWB_2) was analyzed. The results show that the drag behavior at higher C_L (the first test) is quite satisfactory: at $C_L = 0.444$, only 2–3 wave drag counts are added. As for the above second and third off-design conditions, the following analysis demonstrates that there is room for improvement. Specifically, at $M = 0.87$, $C_L = 0.41$ about 17 counts of wave drag were added compared with $M = 0.85$, whereas $C_L^{\max}$ at $M = 0.2$ was equal to 1.47 (compared with $C_L^{\max} = 1.63$ for the initial baseline BWB configuration).

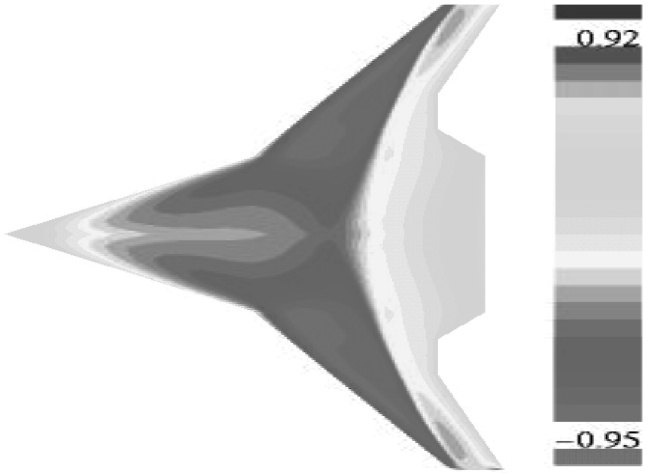

Fig. 12 BWB baseline configuration. Pressure distribution on the aircraft surface at $M = 0.85$, $C_L = 0.41$.

In this connection the following multipoint optimizations were carried out: case BWB_3, which includes the main design point and two secondary design points at high Mach and at takeoff conditions, and case BWB_4, which combines the main design point and the takeoff design point (see Table 1).

Let us consider the results of the three-point optimization. At the main flight conditions, the optimal shape yielded 196.7 counts which is rather close to the theoretical minimum (see the above discussion). The surface pressure distribution on the upper surface of the optimal configuration is compared with this of the baseline geometry in Figs. 12 and 13. It can be assessed that the optimization considerably changed the configuration loading by removing the strong shocks present in the flow over the original aircraft shape. This conclusion can be also confirmed by observation of Figs. 14 and 15, where the streamwise sectional pressure distributions for case BWB_3 are presented.

The off-design performance at higher-than-cruise lift coefficients (at $M = 0.85$) is satisfactory: for example, the drag value at $C_L = 0.45$ is equal to 214.0 counts which means that the additional wave drag (compared with the cruise $C_L = 0.41$) is only about 2–3 aerodynamic counts.

As for the two-point optimization (case BWB_4), the results were as follows: $C_L^{\max}$ increased to 1.671 (thus removing the drawback of case BWB_2 at the takeoff conditions) whereas the total drag at the main design point was equal to 196.6 counts (in fact, preserving the gain in drag value achieved in case BWB_2).

At the same time, the drag value at $M = 0.87$ was even higher than in the one-point optimization of case BWB_2 (216.6 counts

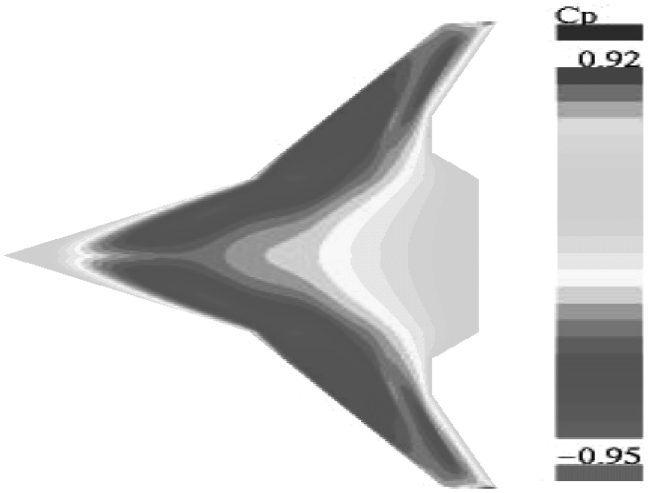

Fig. 13 BWB configuration. Multipoint optimization: case BWB_3. Pressure distribution on the aircraft surface at $M = 0.85$, $C_L = 0.41$.

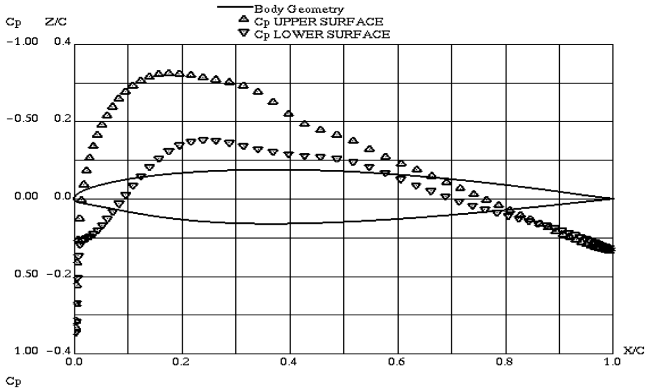

Fig. 14 BWB configuration. Three-point optimization: case BWB_3. Streamwise pressure distribution at section $z = 13.0$ m. $M = 0.85$, $C_L = 0.41$.

compared with 213.4 counts), thus indicating the need for a three-point optimization.

The next important issue is the aerodynamic performance of the optimal shape at high Mach values. As it was already mentioned above, the one- and two-point optimizations resulted in approximately the same value of C_D at $M = 0.87$—about 215.0 counts. The three-point optimization (in which higher-than-cruise Mach flight conditions are additionally taken into account), allows to improve the Mach drag rise characteristics of the BWB aircraft. Specifically, the total drag value at $C_L = 0.41$, $M = 0.87$ became 202.5 counts (a reduction of 12.5 counts compared with the previous optimizations). The analysis of the corresponding pressure distributions (see Figs. 16 and 17) shows that the main mechanism that allowed to reach a significant drag reduction, consists in the successful shock wave destruction.

Alongside surface aerodynamic characteristics, an important source of aerodynamic data needed for the analysis of flow structures, are off-body iso-Mach contours. The corresponding sectional Mach distributions over the baseline configuration and the optimal one (case BWB_3) for the freestream $M = 0.85$ are given in Figs. 18–21.

Already at the symmetry plane, the baseline configuration (see Fig. 18) is characterized by the presence of a supersonic zone which has a tendency to produce the shock wave in the vicinity of 70% of the chord. Contrary to this, the symmetry plane flow over the optimal configuration (Fig. 19) is subsonic, and the sectional loading is shifted in the leading edge direction.

Moving outboard, we note that at $z = 13.0$ m (Fig. 20), the above trend for the baseline configuration has been realized in a strong shock at approximately 55% of the chord length. As this takes place, the height of the corresponding supersonic bell grows and achieves about 35–40% of the local chord length. For the optimal configuration (see Fig. 21), the situation is completely different and the shock wave is absent. Though the supersonic bell is also present,

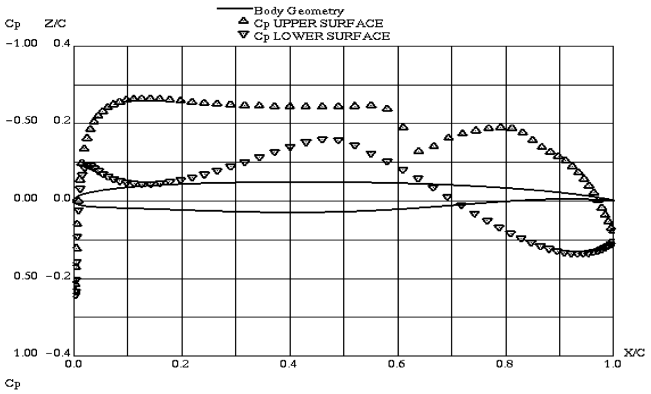

Fig. 15 BWB configuration. Three-point optimization: case BWB_3. Streamwise pressure distribution at section $z = 23.5$ m. $M = 0.85$, $C_L = 0.41$.

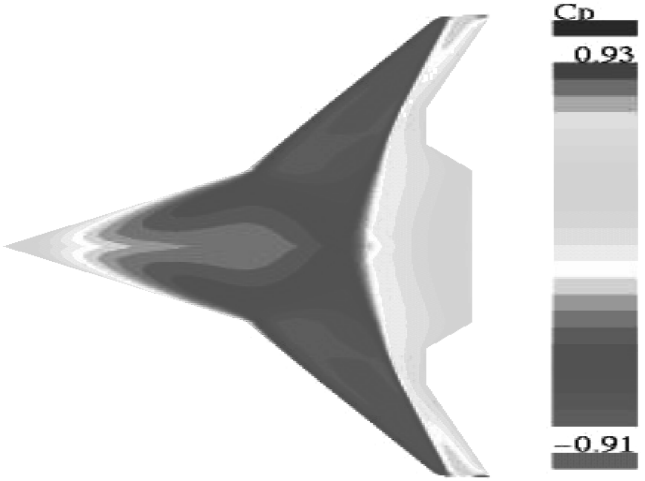

Fig. 16 BWB baseline configuration. Pressure distribution on the aircraft surface at $M = 0.87, C_L = 0.41$.

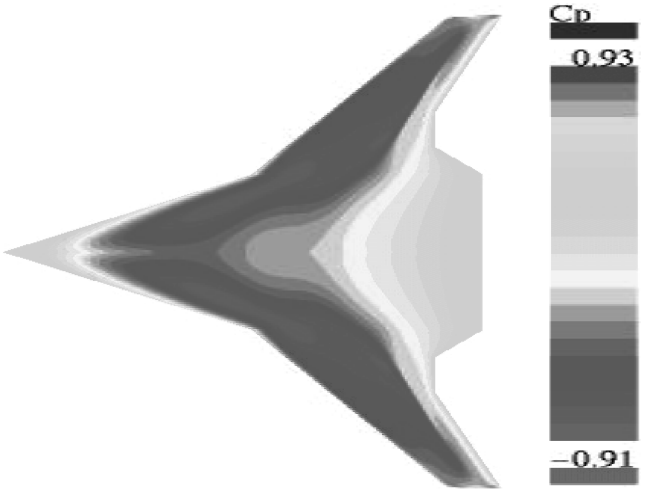

Fig. 17 BWB configuration. Multipoint optimization: case BW_B_3. Pressure distribution on the aircraft surface at $M = 0.87, C_L = 0.41$.

Fig. 18 BWB baseline configuration at $M = 0.85$, $C_L = 0.41$. Mach distribution at symmetry section $z = 0.0$ m.

the transition of the supersonic flow to the subsonic one occurs in a smooth way. Additionally, similar to the symmetry plane, we observe the shift of the sectional loading in the leading edge direction.

To better assess the advantages of different optimization cases, it is interesting to compare the overall aerodynamic performance of the optimized shapes with that of the original aircraft configuration. The

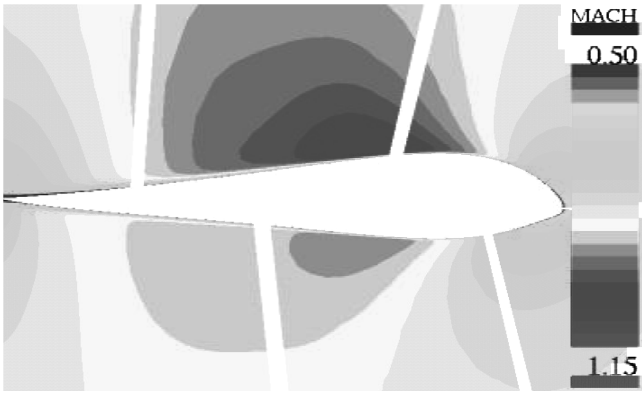

Fig. 19 BWB configuration. Multipoint optimization (case BWB_3) at $M = 0.85, C_L = 0.41$. Mach distribution at symmetry section $z = 0.0$ m.

Fig. 20 BWB baseline configuration at $M = 0.85$, $C_L = 0.41$. Mach distribution at section $z = 13.0$ m.

Fig. 21 BWB configuration. Multipoint optimization (case BWB_3) at $M = 0.85, C_L = 0.41$. Mach distribution at section $z = 13.0$ m.

natural way to do this is to present drag polars at the design freestream Mach numbers $M = 0.85$ and $M = 0.87$, the Mach drag rise curve at the design $C_L = 0.41$ and C_L vs angle of attack curve at $M = 0.20$.

The analysis of drag polars at the main design point (Fig. 22) allows to draw the following conclusions. In all the considered optimization cases, the optimized configurations demonstrate a significant improvement to the original shape in the whole range of lift coefficients. It is important to note that in the wide vicinity of the design lift coefficient, all the polars are very close to each other.

At a higher freestream Mach number, corresponding to a secondary design point at $M = 0.87$, the above mentioned superiority (in terms of drag) of the optimized configurations over the baseline one, is retained for a wide range of C_L values (see Fig. 23). At the same time, contrary to $M = 0.85$, the three-point optimization case BWB_3 has a clear advantage.

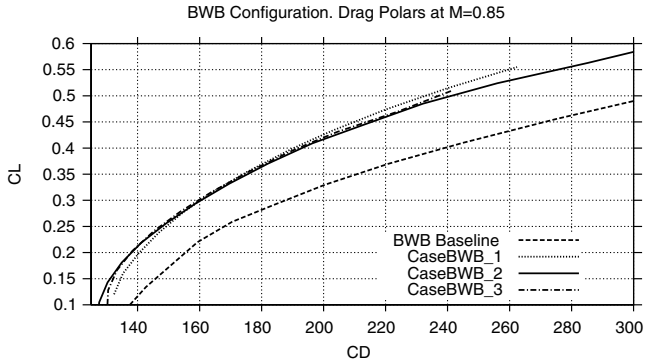

Fig. 22 BWB aircraft. Drag polars at $M = 0.85$. Baseline vs optimal ones.

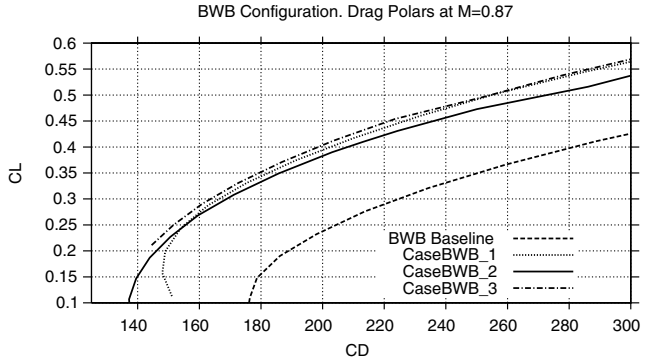

Fig. 23 BWB aircraft. Drag polars at $M = 0.87$. Baseline vs optimal ones.

Let us turn our attention to the analysis of Mach drag rise curves at $C_L = 0.41$ (Fig. 24). Already the original (baseline) shape possesses reasonably good drag rise characteristics: the total drag value is kept practically constant up to $M = 0.80$ with the Mach drag divergence point located close to $M = 0.82$. Nevertheless, the optimization enables one to both decrease the constant level of drag at subsonic and low transonic Mach numbers and to essentially shift the Mach drag divergence point to a higher Mach zone. As this takes place, the value of the Mach drag divergence point for the one- and two-point optimizations is about $M = 0.855$ whereas for the three-point optimization this value is as high as $M = 0.87$.

Summing up the analysis of results for high transonic freestream Mach numbers, it may be concluded that the superiority of the three-point optimization is clearly evident. The final conclusions concerning the feasibility of the optimal shape, may be drawn only upon the aerodynamic performance analysis at the takeoff conditions. The corresponding data may be found in Fig. 25, where C_L vs angle of attack curves at $M = 0.20$ are shown.

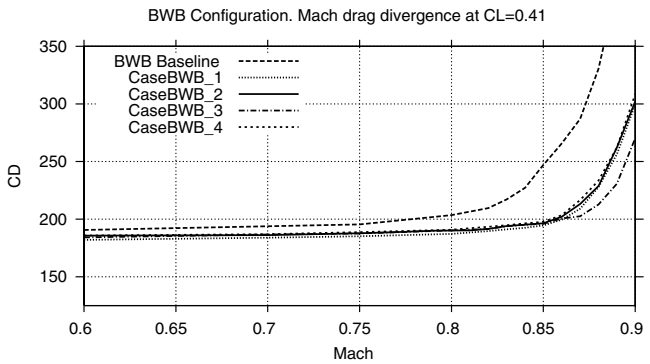

Fig. 24 BWB aircraft. Mach drag divergence at cruise lift coefficient $C_L = 0.41$.

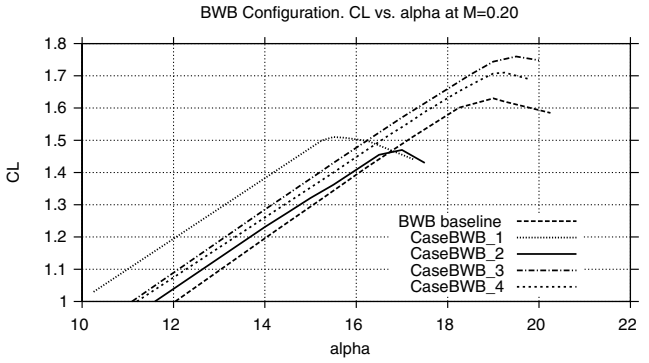

Fig. 25 BWB aircraft. Lift coefficient C_L vs angle of attack at takeoff conditions ($M = 0.20$).

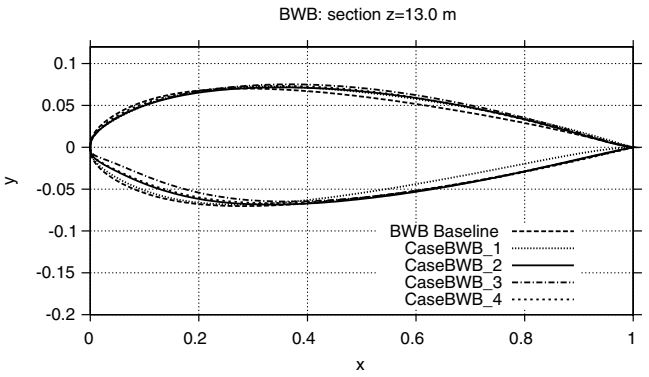

Fig. 26 BWB aircraft. Shape of section at $z = 13.0$ m. Baseline vs optimal ones.

It can be observed that the values of $C_L^{\max}$ for the optimizations case BWB_1 and case BWB_2, where the takeoff requirements were not included into the optimization goals, were lower than that of the baseline configuration. In turn, where the takeoff conditions are taken into account, the corresponding optimizations (case BWB_3 and case BWB_4) produced shapes that visibly improved the baseline $C_L^{\max}$ characteristics.

Finally, based on the above detailed aerodynamic analysis in a wide range of flight conditions, it may be concluded that the three-point optimization possesses the best overall aerodynamic performance.

Let us analyze the connection between the achieved aerodynamic performance of the aircraft and the corresponding optimal shapes. Specifically, it is interesting to reveal the mechanism of drag minimization in terms of geometrical trends in aircraft shape. The optimal shapes (case BWB_1– case BWB_4) vs the baseline geometry at different span stations are depicted in Figs. 26 and 27.

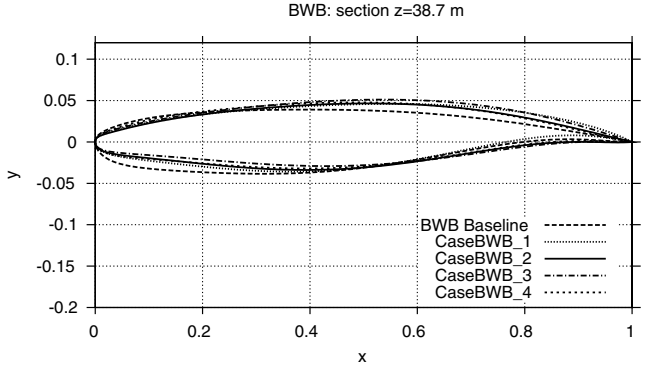

Fig. 27 BWB aircraft. Shape of section at $z = 38.7$ m. Baseline vs optimal ones.

First of all one can see that the optimal shapes, obtained in different optimization conditions, are markedly different. Contrary to this, the corresponding total drag values at the main design point are very close to each other. This leads to a simple but very important conclusion: the considered optimization problem is ill posed. More exactly, this means that small changes in the resulting total drag value may produce significant changes in the corresponding shapes. Practically, essentially different geometrical shapes may yield the same drag value in the small vicinity of the minimum drag. Summing up, it may be concluded: the drag minimization problem has no unique solution.

Mathematically, the ill-posedness of a problem complicates the issue. Practically, the solution of such a problem may produce shapes infeasible from the engineering viewpoint. For example, the optimization may yield an unproducible shape with too small a leading edge radius or a shape that may be practically constructed but is aerodynamically unacceptable due to flight instability.

To remove the above obstacle, we should improve the well-posedness of the problem. In our case, one of the natural and very efficient ways to do this, is to diminish the dimensions of the search space and thus to exclude from consideration the shapes infeasible from the engineering viewpoint. This may be accomplished by introducing numerous geometrical and aerodynamic constraints into the problem. The required constraints can be naturally derived from the multidisciplinary considerations such as flight stability, material requirements and so on.

The presented results show that the imposition of constraints allows one to reach the stated practical goal: to obtain minimum drag configurations and, at the same time, to avoid infeasible shapes. In particular, the optimal shape of case BWB_3 yields the drag value close to the theoretical minimum and complies with the main design requirements coming from the multidisciplinary considerations.

V. Conclusions

The multiconstrained optimization of a blended wing body configuration for minimum total drag has been considered. The important features of the optimization technology included a new strategy for efficient handling of nonlinear constraints in the framework of genetic algorithms, scanning of the optimization search space by a combination of full Navier–Stokes computations with the ROM method, and a multilevel parallelization of the whole computational framework which efficiently makes use of computational power supplied by massively parallel processors. The analysis of a large body of results demonstrates that the developed optimization technique allows for finding the solutions with the performance close to that of the total optimum. The designed shapes that satisfy a large number of aerodynamic and geometrical constraints, are aerodynamically feasible, yield essential aerodynamic improvement to the initial geometry at the main design point alongside good off-design performance. By means of the three-point optimization, we, respectively, achieved 20 and 29% reduction in drag in the main and a higher Mach secondary design points, while keeping $C_L^{\max}$ at the takeoff conditions to the required level.

References

[1] Northrop, J. K., "The Development of All-Wing Aircraft", *Journal of the Royal Aeronautical Society*, Vol. 51, 1947, pp. 481–510.

[2] Portsdam, M. A., Page, M. A., and Liebeck, R. H., "Blended Wing Body Analysis and Design," AIAA Paper 1997-2317, June 1997.

[3] Liebeck, R. H., Page, M. A., and Rawdon, B. K., "Blended Wing Body Subsonic Commercial Aircraft," AIAA Paper 1998-0438, Jan. 1998.

[4] Liebeck, R. H., "Design of the Blended Wing Body Subsonic Transport," *Journal of Aircraft*, Vol. 41, No. 1, 2004, pp. 10–25.

[5] Morris, A. J., "MOB: A European Distributed Multi-Disciplinary Design and Optimization Project," AIAA Paper 2002-5446, Sep. 2002.

[6] Qin, N., Vavalle, A., Le Moigne, A., Laban, M., Hackett, K., and Weierfelt, P., "Aerodynamic Consideration of Blended Wing Body Aircraft," *Progress in Aerospace Sciences*, Vol. 40, No. 6, 2004, pp. 321–343.

[7] Lighthill, M. J., "A New Method of Two-Dimensional Aerodynamic Design," Aeronautical Research Council M&R 1111, 1945.

[8] Bauer, F., Garabedian, P., Korn, D., and Jameson, A., *Supercritical Wing Sections II*, Springer–Verlag, New York, 1975.

[9] Hicks, R. M., and Henne, P. A., "Wing Design by Numerical Optimization," *Journal of Aircraft*, Vol. 15, No. 4, 1978, pp. 407–412.

[10] Anon., "Optimum Design Methods for Aerodynamics," AGARD R-803, 1994.

[11] Jameson, A., "Aerodynamic Design via Control Theory," *Journal of Scientific Computing*, Vol. 3, No. 2, 1988, pp. 233–260.

[12] Jameson, A., "Optimum Aerodynamic Design Using Control Theory," *CFD Review*, Wiley, New York, 1995, pp. 495–528.

[13] Mohammadi, B., and Pironneau, O., *Applied Shape Optimization for Fluids*, Oxford University Press, Oxford, 2001.

[14] Hajela, P., "Nongradient Methods in Multidisciplinary Design Optimization—Status and Potential," *Journal of Aircraft*, Vol. 36, No. 1, 1999, pp. 255–265.

[15] Vicini, A., and Quagliarella, D., "Inverse and Direct Airfoil Design Using a Multiobjective Genetic Algorithm," *AIAA Journal*, Vol. 35, No. 9, 1997, pp. 1499–1505.

[16] Obayashi, S., Yamaguchi, Y., and Nakamura, T., "Multiobjective Genetic Algorithm for Multidisciplinary Design of Transonic Wing Planform," *Journal of Aircraft*, Vol. 34, No. 5, 1997, pp. 690–693.

[17] Epstein, B., and Peigin, S., "Constrained Aerodynamic Optimization of 3-D Wings Driven by Navier–Stokes Computations," *AIAA Journal*, Vol. 43, No. 9, 2005, pp. 1946–1957.

[18] Epstein, B., Rubin, T., and Seror, S., "Accurate Multiblock Navier–Stokes Solver for Complex Aerodynamic Configurations," *AIAA Journal*, Vol. 41, No. 4, 2003, pp. 582–594.

[19] Shu, C.-W., and Osher, S., "Efficient Implementation of Essentially Non-Oscillatory Shock-Capturing Schemes," *Journal of Computational Physics*, Vol. 83, No. 1, 1989, pp. 32–78.

[20] Seror, S., Rubin, T., Peigin, S., and Epstein, B., "Implementation and Validation of the Spalart–Allmaras Turbulence Model for a Parallel CFD Code," *Journal of Aircraft*, Vol. 42, No. 1, 2005, pp. 179–188.

[21] Peigin, S., and Epstein, B., "Robust Handling of Non-Llinear Constraints for GA Optimization of Aerodynamic Shapes," *International Journal for Numerical Methods in Fluids*, Vol. 45, No. 8, 2004, pp. 1339–1362.

[22] Michalewicz, Z., *Generic Algorithms + Data Structures = Evolution Programs*, Springer–Verlag, New York, 1996.

[23] Hoffmeister, F., and Back, T., "Genetic Algorithms and Evolution Strategies: Similarities and Differences," *Proceedings of the 5th Conference on Parallel Problems Solving from Nature*, Springer–Verlag, New York, 1991, pp. 455–469.

[24] Goldberg, D. E., *Genetic Algorithms in Search, Optimization and Machine Learning*, Addison Wesley Longman, Reading, MA, 1989.

[25] Sefrioui, M., Periaux, J., and Ganascia, J. G., "Fast Convergence Thanks to Diversity," *Proceedings of the 5th Annual Conference on Evolutionary Programming*, MIT Press, Cambridge, MA, 1996, pp. 313–321.

[26] Peigin, S., and Epstein, B., "Embedded Parallelization Approach for Optimization in Aerodynamic Design," *Journal of Supercomputing*, Vol. 29, No. 3, pp. 243–263.

A. Messac
Associate Editor